

OmniVaT: Single Domain Generalization for Multimodal Visual-Tactile Learning

Liuxiang Qiu¹, Hui Da², Yuzhen Niu², Tiesong Zhao^{†1}, Yang Cao³, Zheng-Jun Zha³

¹Fujian Key Laboratory for Intelligent Processing and Wireless Transmission of Media Information, College of Physics and Information Engineering, Fuzhou University, Fuzhou 350108, China ²College of Computer and Data Science, Fuzhou University, Fuzhou 350108, China ³MoE Key Laboratory of Brain-inspired Intelligent Perception and Cognition, University of Science and Technology of China, Hefei 230026, China

[†]Corresponding author.

Abstract: Visual-tactile learning (VTL) enables embodied agents to perceive the physical world by integrating visual (VIS) and tactile (TAC) sensors. However, VTL still suffers from modality discrepancies between VIS and TAC images, as well as domain gaps caused by non-standardized tactile sensors and inconsistent data collection procedures. We formulate these challenges as a new task, termed single domain generalization for multimodal VTL (SDG-VTL). In this paper, we propose an OmniVaT framework that, for the first time, successfully addresses this task. On the one hand, OmniVaT integrates a multimodal fractional Fourier adapter (MFFA) to map VIS and TAC embeddings into a unified embedding-frequency space, thereby effectively mitigating the modality gap without multi-domain training data or careful cross-modal fusion strategies. On the other hand, it also incorporates a discrete tree generation (DTG) module that obtains diverse and reliable multimodal fractional representations through a hierarchical tree structure, thereby enhancing its adaptivity to fluctuating domain shifts in unseen domains. Extensive experiments demonstrate the superior cross-domain generalization performance of OmniVaT on the SDG-VTL task.

Project Page: The project page will be released.

MIC@FZU

1 Introduction

Recently, visual-tactile learning (VTL), which leverages both visual (VIS) and tactile (TAC) sensors to enhance robotic perception, has been widely studied for object understanding [14, 37, 12, 43]. However, the absence of standardization in TAC sensor design leads to substantially different imaging mechanisms across sensor families, resulting in drastically varied tactile representations. For example, the real-world GelSight sensor [42] captures gel deformation under object contact using a camera assisted by LED illumination; the simulated Taxim sensor [32] employs a polynomial look-up table to approximate the optical response of the elastomer after deformation; and the Tac3D sensor [45] measures the three-dimensional deformation information using tactile skin and two cameras. Furthermore, even objects within the same category (*e.g.*, metallic objects) exhibit diverse visual appearances due to variations in surface properties and imaging conditions, as shown in fig. 1(a). These discrepancies introduce large modality and domain gaps, making it difficult to establish a unified VIS-TAC feature space. Existing VTL approaches [14, 38, 12] are built upon the assumption that the test domain distribution is subsumed by that of the training domain, which limits their generalization ability to unseen scenarios in the real world. Here, we refer to the VIS-TAC data distribution as a specific domain which is collected by different tactile sensors under different scenarios. For ex-

ample, single-to-single domain methods [14, 38] (as given in fig. 1(b)) exhibit poor generalization ability, as they are evaluated on a test domain sharing the same distribution as the training domain. Prior multiple-to-single domain method [12] train models on multiple VIS-TAC domains and then fine-tune them on a target domain to obtain more effective VIS-TAC representations and mitigate the modality discrepancy, as illustrated in fig. 1(c). However, these approaches require millions of training samples, making data collection and training prohibitively expensive. Motivated by the above challenges, we propose a new single domain generalization for multimodal VTL (SDG-VTL) task, which aims to achieve robust cross-domain VTL.

Single domain generalization (SDG) [4, 26, 52, 36] aims to learn from a single source domain and generalize to multiple unseen domains, achieving impressive results in visual generalization. Though several SDG methods [26, 52] employ adversarial learning to simulate cross-domain representations, they often suffer from unstable convergence and unreliable generation. Other SDG methods [4, 17] adopt metric learning to obtain domain-shared features, yet fail to effectively exploit multimodal cues, leading to suboptimal cross-modal alignment and limited generalization across unseen VIS-TAC domains. Recently, vision-language models [31, 30] have shown remarkable success in improving visual generalization by learning transferable representations from large-scale text-image pairs. However, VIS sensors capture global receptive

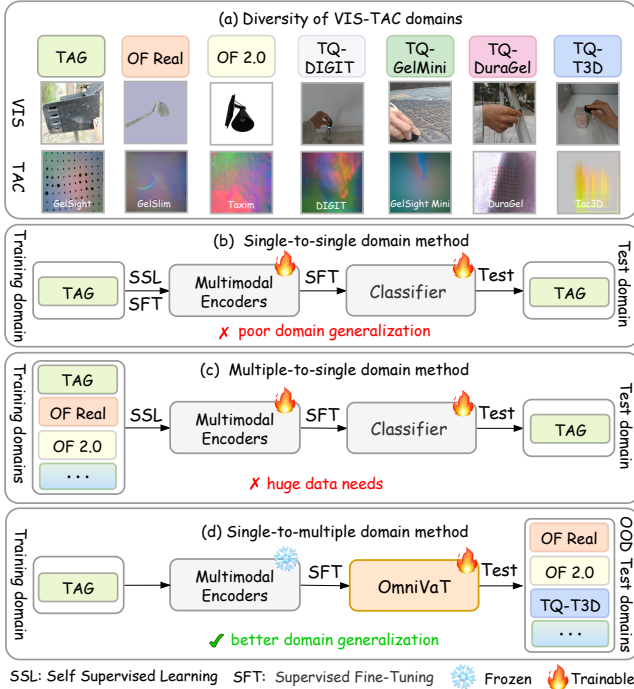


Figure 1 (a) Visualization of various VIS-TAC domains (e.g., metal objects), (b) Single-to-single domain methods [14, 38], (c) Multiple-to-single domain method [12], (d) Our single-to-multiple domain method.

fields, while TAC sensors are inherently local and constrained to contact regions, as shown in fig. 1(a). This large modality gap hinders the effectiveness of existing domain generalization methods when directly applied to cross-domain VTL.

The existing VTL methods usually adopt cross-modal fusion [33, 24, 46] or common feature mapping [38, 9, 12] to mitigate the modality discrepancy. However, these methods address the discrepancy only within a single embedding space, but they fail to learn discriminative decision boundaries for narrowing the modality gap. Several multimodal approaches [53, 7, 49] attempt to alleviate modality discrepancies by mapping features into the frequency domain via Fourier transforms. However, insufficient exploration of the original feature space hinders the discovery of common semantic information across different modalities. Hence, the above single embedding or frequency-based methods may not be effective for achieving a discriminative multimodal feature space, thus failing to reduce the modality gap. Different from embedding or frequency processing, the fractional Fourier transform [51, 41, 6, 22] maps features into a unified embedding-frequency space, providing a more effective perspective for feature projection. This facilitates the mitigation of modality and domain discrepancies among features of the same category.

To address the aforementioned challenges: *modality gap* and *domain gap*, we propose OmniVaT, a novel single VIS-TAC domain generalization framework, which contains a multi-

modal fractional Fourier adapter (MFFA) module and a discrete tree generation (DTG) module. The key novelty of our method lies in the novel formulation of ① *exploiting unified embedding-frequency representations* and ② *expanding diverse and reliable feature nodes* to learn a discriminative and reasonable multimodal feature space, greatly improving the ability of the model to mitigate modality and domain discrepancies. Our main contributions are summarized as follows:

- We observe the co-existence of the modality gap and domain gap in VTL and herein propose a new SDG-VTL task towards real-world applications.
- We are the first to address the SDG-VTL task with a novel OmniVaT framework that incorporates an MFFA module to align VIS-TAC features in a unified embedding-frequency space and a DTG module to discretize fractional representations into a hierarchical tree, thereby mitigating the modality and domain gaps, respectively.
- Our proposed OmniVaT achieves an average accuracy of 66.9% and outperforms existing SOTA methods by at least 13.0% across eight SDG-VTL settings.

2 Related Work

Visual-Tactile Learning (VTL). To mitigate the modality discrepancy between VIS and TAC images, existing VTL methods can be categorized into cross-modal fusion and common feature mapping approaches. Cross-modal fusion-based methods [33, 24, 46] attempt to fuse VIS and TAC modality features to establish cross-modal feature associations, thus reducing the modality discrepancy. For example, Li *et al.*[24] propose an attention-based VIS-TAC fusion network that merges VIS and TAC features to improve recognition performance. Common feature mapping has attracted considerable attention due to its simplicity in achieving modality-shared features by metric learning [38, 9, 12]. For instance, Feng *et al.*[12] attempt to learn a multi-sensor invariant representation through self-supervised learning from huge VIS-TAC data to mitigate the modality gap. However, these methods only mitigate modality discrepancies within a single embedding space and assume identical training-test distributions, thus failing to generalize to unseen scenarios.

Domain Generalization. Domain generalization (DG) focuses on overcoming the domain shift problem, where the data distribution of the target domain differs from that of source domains used for training. Single domain generalization (SDG) [4, 52, 26, 36, 17] aims to achieve domain generalization when only one source domain is available. For example, Xu *et al.*[36] alleviate domain shift by stylization and destylization operations but suffer from unstable convergence and unreliable generation. Gupta *et al.*[17] learn domain-shared features through contrastive learning but fail to fully exploit multimodal cues, resulting in limited gen-

eralization to VIS-TAC domains. Several DG approaches [8, 44, 35] attempt to introduce the vision-language model [31] to extract domain-shared features, yet fail to generalize to unseen TAC domains, which are absent from pre-training data. Frequency-based DG methods [34, 28, 15, 20] employ the Fourier transform for domain-invariant representation but rely on complex fusion between Fourier and embedding spaces. In contrast, the fractional Fourier transform [51, 50, 41, 6, 22] provides a tunable embedding-frequency projection to capture domain-invariant features. Although Zhao *et al.*[50] adopt fractional fusion for spatial-spectral adaptation, their method still requires fine-tuning on target domains and lacks effective alignment to mitigate modality discrepancies in the fractional Fourier space.

Embedding Expansion. To enhance the model’s ability to extract discriminative domain-shared or class-shared features, a series of studies [21, 48, 49] have attempted to generate diverse feature representations through embedding expansion to overcome the domain shift. Ko *et al.*[21] perform linear interpolation expansion between two feature points and generate synthetic points in the embedding space for metric learning. Zhang *et al.*[49] apply convolutional layers to generate diverse amplitude component nuances for visible-infrared person re-identification. The above methods expand in the embedding or frequency space, ignoring that the unified embedding-frequency space can provide a more effective class-invariant feature representation. In addition, the above methods that rely on serial or parallel branches lack an effective mechanism to discretize embedding representations, which limits their ability to simulate various domain shifts.

3 Method

3.1 Formulation of SDG-VTL Task

Existing VTL methods [38, 9, 12] usually assume that the test domain distribution resembles the training distribution. As a result, these methods may suffer from overfitting to seen domain features and fail to effectively recognize objects from unseen VIS-TAC domains due to the diversity of the VIS-TAC domains. Inspired by the widely recognized single domain generalization [26, 52, 36], we introduce the single domain generalization for multimodal VTL (SDG-VTL) task that minimizes the single source VIS-TAC domain \mathcal{S} risk while controlling the worst-case risk over unseen target domains \mathcal{T} , that is

$$\min_{\theta} \sup_{\mathcal{T}: G(\mathcal{S}, \mathcal{T}) \leq \rho} \mathbb{E}_{(x^v, x^t, y) \sim \mathcal{T}} [\ell(\theta; (x^v, x^t, y))], \quad (1)$$

where G is a similarity metric to measure the domain distance and ρ denotes the largest domain discrepancy between \mathcal{S} and \mathcal{T} ; x^v and x^t are VIS and TAC features, respectively; y is the ground-truth label; θ is the parameters of the network; and $\ell(\cdot)$ is the task evaluation (*e.g.*, cross-entropy loss).

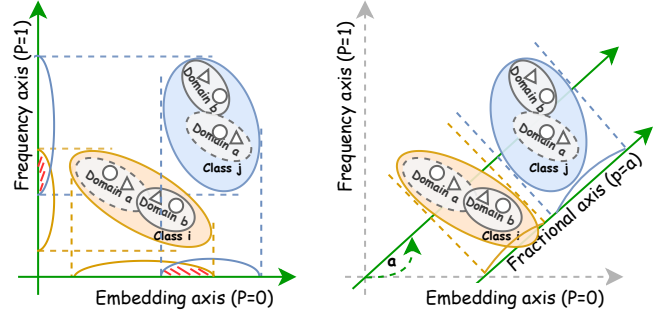


Figure 2 Embedding ($p = 0$) or frequency ($p = 1$) processing causes overlapping projections and inter-class confusion. However, the fractional Fourier transform (FrFT, $p = a$) provides a unified embedding-frequency representation that separates features from different classes more effectively. Circles and triangles represent VIS and TAC features, respectively.

3.2 Motivation

As shown in fig. 1(a), the modality and domain gaps are the main issues that hinder existing domain generalization and VTL methods from effectively learning discriminative features. The fractional Fourier transform (FrFT) [51, 41, 6, 22] allows flexible transformations between embedding and frequency spaces at arbitrary angles, providing a more powerful mechanism for capturing the semantic consistency of representations, as shown in fig. 2. This can be considered an effective approach to achieve class-irrelevant features. The p -th order FrFT of the embedding $\mathbf{E} \in \mathbb{R}^{1 \times D}$, is defined as follows:

$$\text{FrFT}_p(\mathbf{E}(u_0)) = \int_{-\infty}^{\infty} K_p(u_0, u_p) \mathbf{E}(u_0) du_0, \quad (2)$$

where $K_p(u_0, u_p)$ is the kernel function of the fractional Fourier transform; u_0 refers to the original embedding space, and u_p represents the transformed fractional space. **More details about FrFT can be seen in the supplements.**

We then design modules to address modality and domain gaps based on FrFT. For **modality gap**: existing VTL approaches [38, 46], which mainly rely on feature fusion or metric alignment, often suffer from careful module design and insufficient semantic exploitation. Language (LANG) information provides high-level abstract representations of categories that can help the network achieve modality-shared features. Thus, we aim at designing a multimodal fractional Fourier adapter (MFFA) module, which incorporates FrFT to map the VIS-TAC feature into the unified fractional space with the guidance of the LANG information to mitigate the modality discrepancy. LANG information is used only during training because it contains class information and therefore cannot be applied during inference.

For **domain gap**: existing single domain generalization methods typically leverage adversarial learning or feature augmentation to increase the domain diversity. However, due to the instability of the stylization and destylization process, this will

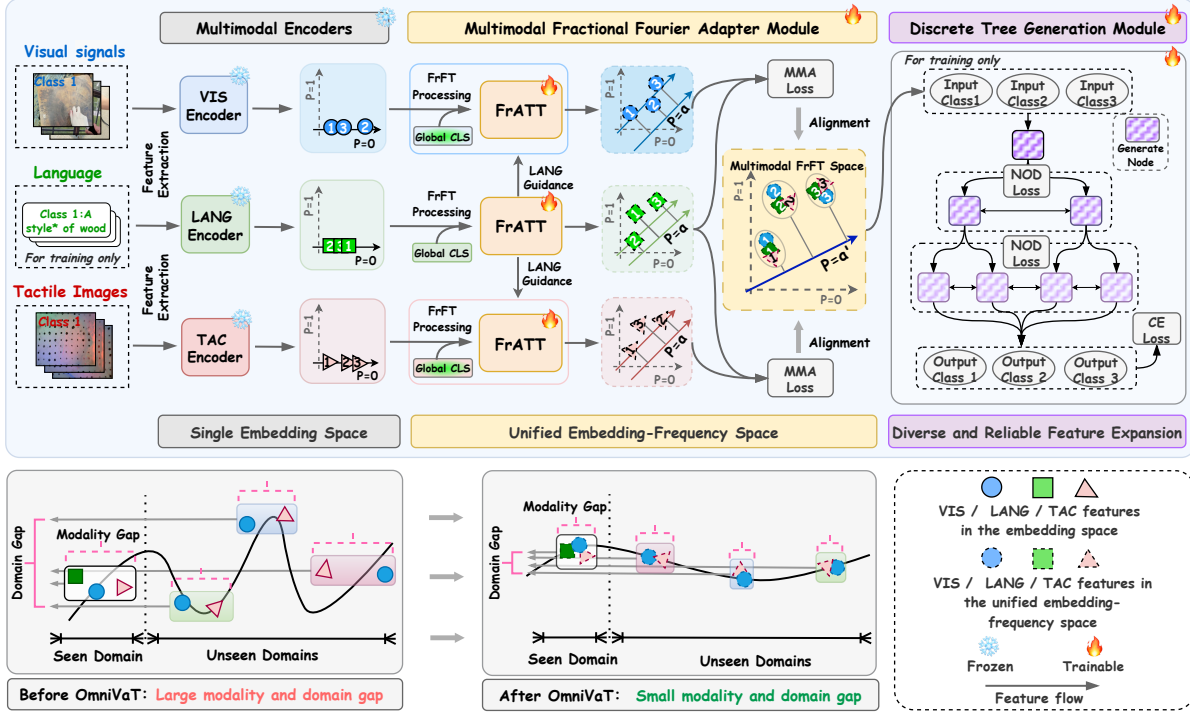


Figure 3 Overview of the proposed OmniVaT, including frozen multimodal encoders, a multimodal fractional Fourier adapter (MFFA) module with the fractional Fourier attention (FrATT) mechanism, and a discrete tree generation (DTG) module. The OmniVaT is jointly optimized by a multimodal alignment (MMA) loss, a node diversity (NOD) loss, and a cross-entropy (CE) loss. The frozen encoders are derived from CLIP [31]. Both the MFFA and DTG modules share the same set of parameters across modalities. Since the LANG embedding contains class information, we use it only during training.

result in the inability to generate reliable features. Though several studies [21, 48, 49] expand embeddings to mitigate domain shift, they follow either serial or parallel expansion designs and struggle to effectively generate diverse feature representations. The tree-based learning methods [40, 29, 39] ensure the continuity of extended features while maintaining the diversity among features, and naturally emerge as an effective solution for learning various feature representations, thereby improving the generalization performance of the model. Based on the above observations, we propose a discrete tree generation (DTG) module to explore and learn a diverse fractional representation set, thereby enhancing the model’s single domain generalization ability to unseen domains.

3.3 Overview of Proposed OmniVaT

The overview of our proposed OmniVaT is shown in fig. 3. OmniVaT consists of frozen VIS, TAC, and LANG encoders, an MFFA module, and a DTG module, respectively. We adopt PromptStyler [8] to generate the missing language information (e.g., “A style* of [Class]”).

3.4 Multimodal Fractional Fourier Adapter (MFFA) Module

Suppose that we have the single source VIS-TAC domain $\mathcal{D}_s = \{x_i^v, x_i^t, y_i\}_{i=1}^N$ with auxiliary LANG information x_i^l , where N represents number of samples. After passing through the frozen VIS encoder, TAC encoder, and LANG encoder, we obtain the VIS embedding $\mathbf{E}^v \in \mathbb{R}^{1 \times D}$, TAC embedding $\mathbf{E}^t \in \mathbb{R}^{1 \times D}$, and LANG embedding $\mathbf{E}^l \in \mathbb{R}^{1 \times D}$, respectively. Here, D is the dimension of the embedding. To reduce the modality gap, we propose the MFFA module, which maps VIS and TAC embeddings into a fractional embedding-frequency space with the guidance of the LANG information by the cross-modal fractional Fourier attention mechanism, and further mitigates modality discrepancies through the multimodal alignment loss. This module eliminates the need for careful cross-modal fusion design while enabling more comprehensive information mining across modalities. Firstly, we introduce the FrFT processing to map the LANG embedding into the unified fractional space, that is

$$\begin{aligned} \mathbf{F}^l &= \text{FrFT Processing}(\mathbf{E}^l) \\ &= \mathcal{U}(\mathcal{R}(\text{FrFT}_p(\theta_{e,l} \mathbf{E}^l))) + j \mathcal{U}(\mathcal{I}(\text{FrFT}_p(\theta_{e,l} \mathbf{E}^l))), \end{aligned} \quad (3)$$

where $\theta_{e,l} \in \mathbb{R}^{E \times 1}$ are trainable parameters that expand the embedding dimensionality, $\text{FrFT}_p(\cdot)$ is the p -th order frac-

tional Fourier transform operation; $\mathcal{R}(\cdot)$ and $\mathcal{I}(\cdot)$ denote the real and imaginary part operators, respectively; $\mathcal{U}(\cdot)$ means the ReLU operation; j is the imaginary unit.

Then, we propose a fractional Fourier attention (FrATT) mechanism to achieve the encoded fractional LANG representation, which can be written as:

$$\begin{aligned}\bar{\mathbf{F}}^l &= \text{FrATT}(\mathbf{F}^l, \mathbf{F}_g^l \oplus \mathbf{F}^l) \\ &= \text{FFN}(\text{Mean}(\frac{\text{SM}(\theta_Q \mathbf{F}^l \theta_K (\mathbf{F}_g^l \oplus \mathbf{F}^l)^T)}{\sqrt{D}} \theta_V (\mathbf{F}_g^l \oplus \mathbf{F}^l))),\end{aligned}\quad (4)$$

where global class (CLS) token $\mathbf{F}_g^l \in \mathbb{R}^{1 \times D}$ means the average representation of the same class of the input \mathbf{F}^l in the mini-batch which can get the global information of class to overcome intra-class variations; \oplus denotes the broadcast addition operation; $\theta_Q \in \mathbb{R}^{D \times D}$, $\theta_K \in \mathbb{R}^{D \times D}$, and $\theta_V \in \mathbb{R}^{D \times D}$ are linear layers to project the \mathbf{F}^l and $(\mathbf{F}_g^l \oplus \mathbf{F}^l)$ into query space, key, and value space, respectively; $\text{SM}(\cdot)$ and $\text{Mean}(\cdot)$ denote the Softmax and mean operations, respectively. $\text{FFN}(\cdot)$ is the fully connected feedforward network. Subsequently, guided by the LANG feature $\bar{\mathbf{F}}^l$, we further project the VIS embedding \mathbf{E}^v into the unified embedding-frequency feature space to achieve modality-invariant representations, that is

$$\mathbf{F}^v = \text{FrFT Processing}(\theta_{e,v}(\bar{\mathbf{F}}^l + \mathbf{E}^v)), \quad (5)$$

where $\theta_{e,v} \in \mathbb{R}^{E \times 1}$ is the trainable parameters that extend the number of embedding. We further adopt the FrATT mechanism to establish semantic correlations among different modalities, as follows

$$\bar{\mathbf{F}}^v = \text{FrATT}(\bar{\mathbf{F}}^l, \mathbf{F}_g^v \oplus \mathbf{F}^v). \quad (6)$$

Similarly to eqs. (5) and (6), we can also obtain the fractional TAC feature $\bar{\mathbf{F}}^t$ after language guidance and the FrATT mechanism. To better optimize the fractional order in the embedding-frequency space, we align the representations between VIS, TAC, and LANG features to reduce the modality gap by the multimodal alignment (MMA) loss

$$\mathcal{L}_{\text{MMA}} = \lambda(D_{\text{KL}}(\bar{\mathbf{F}}^l, \bar{\mathbf{F}}^v) + D_{\text{KL}}(\bar{\mathbf{F}}^l, \bar{\mathbf{F}}^t)), \quad (7)$$

where $D_{\text{KL}}(\cdot)$ denotes the Kullback-Leibler (KL) divergence function, λ adjusts the contribution of KL divergence. After the MFFA module, we can efficiently and effectively exploit the associations among different modality embeddings in the unified embedding-frequency space, thus greatly mitigating the modality discrepancy.

3.5 Discrete Tree Generation (DTG) Module

To reduce the domain shift, we propose a DTG module, which hierarchically expands diverse and reliable features in the unified embedding-frequency space with a tree structure. Specifically, given an input unified embedding-frequency VIS-TAC-LANG feature \mathbf{T} (*i.e.*, $\bar{\mathbf{F}}^v + \bar{\mathbf{F}}^t + \bar{\mathbf{F}}^l$), we construct a binary

tree where each node corresponds to an expanded feature. The child nodes are generated through a linear transformation function $\mathcal{F}(\cdot)$ applied to the parent node, allowing multi-level expansion. Formally, the expansion process at layer r can be written as

$$\mathbf{T}_{m,n}^{(r+1)} = \mathcal{F}(\mathbf{T}_m^{(r)}, \mathbf{W}_{m,n}^{(r)}), \quad (8)$$

where $\mathbf{T}_m^{(r)}$ denotes the m -th parent feature node at layer $r = \{1, \dots, R-1\}$ and R is the depth of the tree; $\mathbf{W}_{m,n}^{(r)} \in \mathbb{R}^{D \times D}$ are learnable parameters for the n -th child node of m -th parent node. By recursively applying $\mathcal{F}(\cdot)$, we obtain an expanded fractional feature set of each layer $\mathbf{T}^{\text{tree}} = \{\mathbf{T}_m^{(r)}\}$. To further enhance feature diversity and prevent redundancy among expanded nodes, we introduce node diversity (NOD) loss as a regularization term. By minimizing NOD loss (*i.e.*, reducing the cosine similarity between different node representations), we encourage their independence and thus achieve a more dispersed exploration of the feature space. Concretely, the cosine similarity $\mathbf{A}_{i,j}^{(r)}$ between i -th node $\mathbf{T}_i^{(r)}$ and j -th node $\mathbf{T}_j^{(r)}$ at layer r can be computed as

$$\mathbf{A}_{i,j}^{(r)} = \frac{\mathbf{T}_i^{(r)\top} \mathbf{T}_j^{(r)}}{\ell_2(\mathbf{T}_i^{(r)}) \ell_2(\mathbf{T}_j^{(r)})}, \quad (9)$$

where $\ell_2(\cdot)$ means L2-normalization operation. We incorporate the NOD loss to hierarchically discretize node representation at different layers, as follows

$$\mathcal{L}_{\text{NOD}} = \sum_{r=1}^R \|\mathbf{A}^{(r)} - \mathbf{I}^{(r)}\|_F. \quad (10)$$

where $\mathbf{I}^{(r)}$ is the identity matrix and whose shape is $2^{r-1} \times 2^{r-1}$; $\|\cdot\|_F$ denotes the Frobenius norm that provides stable gradients and facilitates more reliable optimization. The NOD loss promotes a structured and progressive disentanglement of node features, and the domain representation enhanced VIS and TAC features, *i.e.*, $\hat{\mathbf{F}}^v$ and $\hat{\mathbf{F}}^t$, that is

$$\hat{\mathbf{F}}^v = \text{Mean}(\mathbf{T}^{\text{tree}}) + \bar{\mathbf{F}}^v, \hat{\mathbf{F}}^t = \text{Mean}(\mathbf{T}^{\text{tree}}) + \bar{\mathbf{F}}^t. \quad (11)$$

In this way, the proposed DTG module enables a structured and progressive exploration of diverse feature spaces, producing robust modality-invariant representations while avoiding the oversimplified parallel expansion of previous embedding-based approaches. The joint loss is defined as

$$\mathcal{L} = \mathcal{L}_{\text{MMA}} + \mathcal{L}_{\text{NOD}} + \mathcal{L}_{\text{CE}}, \quad (12)$$

where \mathcal{L}_{CE} represents the cross-entropy loss.

4 Experiments

More details on datasets, task settings, ablation studies, and comparison results are provided in the supplements.

Table 1 Comparison with state-of-the-art methods on the SDG-VTL across eight VIS-TAC domains. “S” / “T” means the source / target domain, and “→ X” represents the evaluation of the other unseen target domains, excluding the seen source domain. \diamond and \boxtimes denote original TAC learning and VTL methods, respectively. The best results are marked with **Bold**. Δ LDC denotes the improvements of the proposed OmniVaT over LDC. The metrics are accuracy (ACC, %) and Macro-F1 (F1*, %), respectively.

Methods / Venue	S: TAG	S: OF Real	S: OF 2.0 A	S: OF 2.0 B	S: TQ-DIGIT	S: TQ-GelMini	S: TQ-DuraGel	S: TQ-T3D	Average
	T: → X								
	ACC / F1*								
SITR \diamond / ICLR-25 [17]	33.1 / 16.7	25.3 / 14.7	34.7 / 19.8	20.1 / 9.7	30.6 / 16.8	33.6 / 33.6	34.1 / 22.3	38.4 / 25.5	31.2 / 19.9
VT CMC \boxtimes / NeurIPS-22 [38]	31.5 / 10.7	25.8 / 9.8	33.9 / 6.3	32.9 / 5.7	36.0 / 21.4	28.5 / 13.1	31.7 / 19.2	15.5 / 7.3	29.5 / 11.7
RobustVisH \boxtimes / MM-25 [46]	32.7 / 17.9	30.9 / 10.8	32.9 / 11.6	32.5 / 11.5	27.1 / 10.4	27.5 / 10.7	28.1 / 11.9	23.5 / 9.7	29.4 / 11.8
<i>ResNet-50 [18] with pre-trained weights from CLIP [31]</i>									
CLIP / ICML-21 [31]	40.7 / 33.4	41.4 / 34.8	40.6 / 34.5	40.6 / 34.5	39.1 / 30.2	39.8 / 30.2	38.7 / 30.2	29.6 / 22.5	38.8 / 31.3
PromptStyler / ICCV-23 [8]	48.7 / 37.3	36.3 / 25.3	45.5 / 38.7	34.9 / 29.8	44.4 / 35.5	46.1 / 38.4	45.0 / 39.3	47.0 / 31.8	43.5 / 34.5
SPG / ECCV-24 [1]	47.9 / 43.3	42.8 / 38.7	45.2 / 42.9	38.5 / 29.7	58.7 / 52.5	56.4 / 54.7	55.2 / 51.0	47.1 / 35.6	49.0 / 43.6
LDC / CVPR-25 [25]	43.9 / 33.3	43.2 / 32.7	44.8 / 33.8	52.3 / 43.7	38.3 / 22.0	37.1 / 22.6	39.4 / 25.6	43.9 / 27.9	42.9 / 30.2
OmniVaT / Ours	52.0 / 49.7	51.6 / 50.0	52.4 / 52.3	53.0 / 55.2	59.1 / 54.6	57.6 / 52.7	58.4 / 52.9	52.4 / 39.8	54.6 / 50.9
Δ LDC	8.1 / 16.4	8.4 / 17.3	7.6 / 18.5	0.7 / 11.5	20.8 / 32.6	20.5 / 30.1	19.0 / 27.3	8.5 / 11.9	11.7 / 20.7
<i>ViT-B / 16 [11] with pre-trained weights from CLIP [31]</i>									
CLIP / ICML21 [31]	47.8 / 40.0	48.2 / 40.1	47.8 / 41.1	47.8 / 41.1	48.3 / 36.7	46.5 / 37.4	46.5 / 35.0	42.6 / 30.8	46.9 / 37.8
PromptStyler / ICCV-23 [8]	51.7 / 40.6	42.3 / 30.1	48.9 / 41.2	38.0 / 26.7	54.3 / 47.2	47.0 / 39.8	51.8 / 48.1	49.4 / 30.9	47.9 / 38.1
SPG / ECCV-24 [1]	49.4 / 41.9	49.8 / 42.0	49.1 / 42.8	49.4 / 42.0	53.1 / 46.9	53.8 / 48.6	51.6 / 46.3	50.4 / 43.8	50.8 / 44.3
MMRL / CVPR-25 [16]	46.0 / 33.5	45.9 / 45.4	42.9 / 30.1	42.3 / 37.2	36.0 / 17.9	27.3 / 15.2	29.6 / 14.4	48.8 / 34.8	39.9 / 28.6
LDC / CVPR-25 [25]	50.1 / 36.3	49.5 / 37.6	52.2 / 43.9	52.2 / 43.8	53.8 / 38.9	44.7 / 35.3	49.2 / 38.3	52.9 / 34.9	50.6 / 38.6
OmniVaT / Ours	56.2 / 53.7	58.4 / 56.5	58.6 / 58.2	61.2 / 60.3	56.4 / 50.1	57.3 / 53.5	56.3 / 51.8	54.1 / 47.9	57.3 / 54.0
Δ LDC	6.1 / 17.4	8.9 / 18.9	6.4 / 14.3	9.0 / 16.5	2.6 / 11.2	12.6 / 18.2	7.1 / 13.5	1.2 / 13.0	6.7 / 15.4
<i>ViT-L / 14 [11] with pre-trained weights from CLIP [31]</i>									
CLIP / ICML-21 [31]	48.7 / 42.6	48.9 / 42.8	49.8 / 44.8	49.8 / 44.8	48.9 / 39.3	46.7 / 38.3	46.1 / 37.9	39.7 / 30.7	47.3 / 40.1
PromptStyler / ICCV-23 [8]	54.4 / 47.6	42.6 / 34.9	49.8 / 47.1	44.7 / 35.6	55.5 / 46.7	54.3 / 46.4	54.6 / 49.4	49.8 / 33.3	50.7 / 42.6
SPG / ECCV-24 [1]	57.5 / 54.5	53.6 / 49.7	47.8 / 39.8	39.0 / 31.9	61.0 / 53.4	55.7 / 49.3	65.0 / 61.8	51.9 / 46.3	53.9 / 48.3
MMRL / CVPR-25 [16]	59.5 / 54.6	35.2 / 35.1	34.3 / 22.9	44.6 / 39.4	40.6 / 41.4	33.3 / 22.8	30.1 / 19.6	51.2 / 43.2	41.1 / 34.9
LDC / CVPR-25 [25]	55.2 / 45.5	49.2 / 43.2	52.7 / 43.5	55.3 / 46.7	53.9 / 38.9	53.6 / 42.0	55.3 / 41.6	53.5 / 35.2	53.6 / 42.1
OmniVaT / Ours	62.6 / 64.1	64.9 / 65.8	67.4 / 68.0	67.2 / 68.5	68.5 / 65.9	68.8 / 67.2	70.1 / 66.8	65.4 / 58.0	66.9 / 65.5
Δ LDC	7.4 / 18.6	15.7 / 22.6	14.7 / 24.5	11.9 / 21.8	14.6 / 27.0	15.2 / 25.2	14.8 / 25.2	11.9 / 22.8	13.3 / 23.4

4.1 Experimental Settings

1) Datasets and evaluation metrics: We collect VIS-TAC images from four datasets (*i.e.*, Touch-and-Go (TAG) [38], ObjectFolder (OF) Real [13], ObjectFolder (OF) 2.0 [14], and TacQuad (TQ) [12]) spanning 8 distinct domains (*i.e.*, TAG, OF Real, OF 2.0 A, OF 2.0 B, TQ-DIGIT, TQ-GelMini, TQ-DuraGel, and TQ-T3D), that share five common material categories (*i.e.*, wood, steel, plastic, ceramic, and glass). We train on a single source domain and evaluate on the remaining unseen target domains, reporting the average top-1 accuracy (ACC) and Macro-F1 (F1*) over three random seeds.

2) Implementation Details: During the training step, VIS and TAC images are resized to $3 \times 224 \times 224$ and augmented by the random horizontal flip and the feature normalization. We choose the publicly available pre-trained model CLIP [31] as our frozen VIS, TAC, and LANG encoders. VIS and the TAC encoders are implemented with ResNet-50 [18], ViT-B/16 [11], or ViT-L/14 [11], the LANG encoder is adopted by Transformer in experiments. The dimensions of each LANG, VIS, and TAC embedding are $D = 1024 / 512 / 768$ when VIS and the TAC encoders are implemented with ResNet-50 / ViT-B/16 / ViT-L/14, respectively. The fractional order p , extension parameter E , balance weight λ , and depth R of the tree are set to 0.5, 4, 10, and 3 in the FrFT and DTG modules, respectively. As PromptStyler [8], we generate the 80 LANG samples for each class. For each mini-batch, 16 paired VIS-TAC samples with auxiliary LANG information are randomly

Table 2 Cosine similarity margins of different multimodal learning methods which are trained on TAG and tested on the unseen OF Real, OF 2.0 A, and TQ-T3D domains.

Methods	OF Real	OF 2.0 A	TQ-T3D	[OF Real; TQ-T3D]	[OF 2.0 A; TQ-T3D]
CLIP [31]	0.036	0.075	0.033	0.007	0.006
PromptStyler [8]	0.034	0.061	0.035	0.013	0.017
SPG [1]	0.029	0.050	0.026	0.016	0.020
MMRL [16]	0.016	0.030	0.022	0.008	0.015
LDC [25]	0.041	0.040	0.046	0.028	0.017
OmniVaT	0.168	0.258	0.218	0.191	0.143

selected. We introduce the cosine annealing warm-up strategy [27] to update the learning rate, and the initial learning rate is set to 0.05. OmniVaT is optimized by stochastic gradient descent with a momentum of 0.9 and trained for 20 epochs, implemented in PyTorch on an NVIDIA RTX 3090 GPU.

4.2 Comparison with State-of-the-Art Methods

1) Effectiveness of SDG-VTL: table 1 shows that, compared with previous common feature mapping VTL method (*i.e.*, VT CMC [38]), the proposed OmniVaT improves the recognition accuracy by 20.5% on the TAG → X task. OmniVaT also achieves the Macro-F1 of 50.0%, about 39.0% higher than RobustVisH [46] which introduces cross-modal fusion to integrate multimodal features on the OF Real → X task. Although SITR [17] aims to learn sensor-invariant representa-

Table 3 All methods are trained and tested on a single NVIDIA RTX 3090 GPU using the TAG domain. Trainable parameters (M), training time (s/epoch) on the TAG dataset, GPU memory (MB), inference speed (FPS), accuracy (ACC, %), and Macro-F1 (F1*, %) are reported. TAG \rightarrow X means that the methods are trained on the TAG domain and tested on the other unseen domains. \ddagger means that we reduce the feature dimension to 64. CLIP [31] is the zero-shot method.

Methods / Venue	Trainable Parameters	Training Time	GPU Memory	Inference Speed	TAG \rightarrow X ACC / F1*	OF 2.0 A \rightarrow X ACC / F1*
<i>ViT-B / 16 [11] with pre-trained weights from CLIP [31]</i>						
CLIP / ICML-21 [31]	-	-	1,158	188.2	47.8 / 40.0	47.8 / 41.1
PromptStyler / ICCV-23 [8]	0.3	34.1	2,555	156.8	51.7 / 40.6	48.9 / 41.2
SPG / ECCV-24 [1]	4.7	23,180.2	4,936	91.1	49.4 / 41.9	49.1 / 42.8
MMRL / CVPR-25 [16]	5.0	58.3	3,603	163.3	46.0 / 33.5	42.9 / 30.1
LDC / CVPR-25 [25]	3.4	23.2	2,011	172.5	50.1 / 36.3	52.2 / 43.9
OmniVaT / Ours	5.1	141.9	2,845	75.2	56.2 / 53.7	58.6 / 58.2
OmniVaT \ddagger / Ours	0.2	98.4	2,779	111.1	55.0 / 54.1	56.3 / 55.1

tions through pre-training on large-scale simulated TAC data, our proposed OmniVaT surpasses Sitr at least by 17.7% in accuracy when trained on the simulated to real-world scenarios (e.g., OF 2.0 A \rightarrow X). table 1 also shows that our OmniVaT outperforms the previous multimodal learning methods MMRL [16] and LDC [25] by about 13.0% Macro-F1 with pre-trained ViT-B/16 on TQ-T3D \rightarrow X task. On the TQ-DuraGel \rightarrow X task, OmniVaT outperforms SPG [1] which relies on the generative model to obtain class-invariant features by 4.7% in accuracy with pre-trained ViT-B/16. Under the ViT-L/14 setting, our OmniVaT achieved the best average accuracy and Macro-F1 across 8 domains, reaching 66.9% and 65.5%, respectively. The above experimental results demonstrate that our OmniVaT can effectively mitigate modality and domain gaps, achieving efficient single domain generalization for VTL.

To further evaluate the effectiveness of different methods on the TAG \rightarrow X task, we randomly sample 657,000, 657,000, 308,025, 499,500, and 499,500 intra-class/inter-class pairs from the unseen OF Real, OF 2.0 A, TQ-T3D, [OF Real; TQ-T3D], and [OF 2.0 A; TQ-T3D] domains, respectively, and report the cosine similarity margin [5], as shown in table 2. Here, [;] denotes the concatenation of two unseen domains. Our OmniVaT achieves the largest cosine-similarity margins, reaching 0.191 and 0.143 on the unseen [OF Real; TQ-T3D] and [OF 2.0 A; TQ-T3D] domains, respectively. These results demonstrate that our OmniVaT effectively reduces modality and domain gaps across unseen domains, thereby enhancing cross-domain generalization.

2) Computational Cost: table 3 summarizes the trainable parameters (M), training time (s/epoch) on the TAG dataset, GPU memory (MB), inference speed (measured in frames per second with a batch size of 16, FPS), accuracy (ACC, %), and Macro-F1 (F1*, %) on the single domain generalization TAG \rightarrow X task for each approach. As shown in table 3, OmniVaT reduces the training time by 23,038.3 seconds compared with SPG [1], while improving the accuracy from 49.4% to 56.2%. Notably, the TAC sensor usually captures tactile images at 30 FPS and OmniVaT reaches an inference speed of 75.2 FPS,

Table 4 The influence of the multimodal VIS-TAC image representation learning on the TAG \rightarrow X task. The metrics are accuracy (ACC, %) and Macro-F1 (F1*, %).

Methods	Training Modalities	Test Modalities	TAG \rightarrow X
	<i>ViT-B / 16 [11] with pre-trained weights from CLIP [31]</i>		
	LANG / VIS / TAC	VIS / TAC	ACC / F1*
MMRL [16]	- / \checkmark / -	\checkmark / -	14.4 / 5.5
	- / \checkmark / \checkmark	\checkmark / \checkmark	14.3 / 5.5
	\checkmark / \checkmark / -	\checkmark / -	51.0 / 42.6
	\checkmark / \checkmark / \checkmark	\checkmark / \checkmark	46.0 / 33.5
LDC [25]	- / \checkmark / -	\checkmark / -	46.8 / 34.4
	- / \checkmark / \checkmark	\checkmark / \checkmark	42.5 / 26.7
	\checkmark / \checkmark / -	\checkmark / -	52.9 / 43.5
	\checkmark / \checkmark / \checkmark	\checkmark / \checkmark	50.1 / 36.3
OmniVaT (Ours)	- / \checkmark / -	\checkmark / -	53.0 / 48.1
	- / \checkmark / \checkmark	\checkmark / \checkmark	54.5 / 48.0
	\checkmark / \checkmark / -	\checkmark / -	54.9 / 51.8
	\checkmark / \checkmark / \checkmark	\checkmark / \checkmark	56.2 / 53.7

demonstrating its suitability for real-time deployment. To assess OmniVaT’s performance in resource-limited conditions, we reduce the representation dimensionality from 512 to 64. The lightweight OmniVaT \ddagger not only reduces the number of trainable parameters by 0.1M, 4.5M, 4.8M, and 3.2M compared to PromptStyler [8], SPG [1], MMRL [16], and LDC [25], respectively, but also achieves the impressive 54.1% Macro-F1 on the TAG \rightarrow X task. These experiments demonstrate that our OmniVaT effectively achieves a compelling balance between computational efficiency and performance.

4.3 Ablation Studies

1) Effectiveness of Multimodal VTL: As shown in table 4, compared to single VIS modality generalization, our OmniVaT effectively reduces the modality discrepancy and improves generalization performance by 1.9% Macro-F1 on the generalization tasks of TAG \rightarrow X with training LANG information. These results indicate that the proposed OmniVaT effectively mitigates the discrepancies between different modalities and improves domain generalization. Although previous vision-language methods [16, 25] achieve good generalization with a single VIS modality, they struggle to handle

Table 5 The influence of key components of the proposed OmniVaT on the TAG \rightarrow X and OF 2.0 A \rightarrow X tasks, respectively. The metrics are accuracy (ACC, %) and Macro-F1 (F1*, %).

#	Methods	TAG \rightarrow X	OF 2.0 A \rightarrow X
		ACC / F1*	ACC / F1*
1	Baseline + \mathcal{L}_{CE}	51.7 / 40.6	48.9 / 41.2
2	+MFFA (w/o \mathcal{L}_{MMA})	54.5 / 51.2	51.4 / 54.6
3	+MFFA	54.8 / 52.5	56.9 / 56.2
4	+DTG (w/o \mathcal{L}_{NOD})	53.2 / 48.0	53.8 / 52.1
5	+DTG	53.6 / 49.8	54.9 / 54.6
6	+MFFA+DTG	56.2 / 53.7	58.6 / 58.2

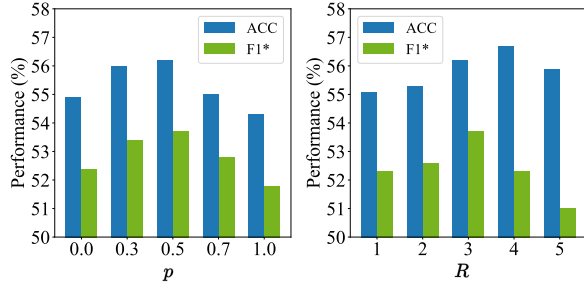


Figure 4 The influence of the fractional order p and the depth R of tree on the TAG \rightarrow X task. When $p = 0.0$ or 1.0 , it is fixed; otherwise, it is learnable.

the VIS-TAC modality discrepancy, leading to a decline in generalization performance.

2) Effectiveness of Key Components: As shown in table 5, we evaluate the effectiveness of the key components of the proposed OmniVaT, which is composed of an MFFA module and a DTG module. We train the proposed modules on the TAG \rightarrow X and OF 2.0 A \rightarrow X tasks, respectively. Method 1 represents the Baseline [8] method with pre-trained ViT-B/16 [11] weights from CLIP [31]. By incorporating MFFA without the MMA loss (+MFFA w/o \mathcal{L}_{MMA}), Method 2 achieves a 10.6% Macro-F1 improvement over the Baseline on the TAG \rightarrow X task, indicating that MFFA enables effective multimodal embedding interactions in a unified embedding-frequency space through FrATT. When the MMA loss is introduced, Method 3 achieves 56.2% Macro-F1 on the OF 2.0 A \rightarrow X task, showing that \mathcal{L}_{MMA} further enhances VIS-TAC alignment and mitigates modality discrepancy. Similarly, Compared with Method 1, adding DTG without the NOD loss (+DTG w/o \mathcal{L}_{NOD}) brings a 1.5% accuracy increase on the TAG \rightarrow X. Method 5 (+DTG) further improves Macro-F1 by 1.8% over Method 4 on the TAG \rightarrow X task, demonstrating that DTG effectively diversifies fractional representations for single domain generalization. Finally, combining MFFA and DTG (Method 6) yields +1.7% accuracy and +2.0% Macro-F1 over Method 3 on OF 2.0 A \rightarrow X task, confirming that OmniVaT effectively reduces modality discrepancy and enhances domain generalization.

3) Effectiveness of the Tree Generation: To evaluate the influence of our discrete tree generation (DTG), we replace

Table 6 The influence of the different feature generation methods on the source TAG and OF 2.0 A domains, respectively. The metrics are accuracy (ACC, %) and Macro-F1 (F1*, %).

Methods	TAG \rightarrow X	OF 2.0 A \rightarrow X
	ACC / F1*	ACC / F1*
Baseline	51.7 / 40.6	48.9 / 41.2
OmniVaT (linear interpolation)	54.6 / 51.5	56.5 / 56.2
OmniVaT (series generation)	55.3 / 52.3	56.9 / 56.6
OmniVaT (parallel generation)	55.0 / 51.8	57.3 / 57.4
OmniVaT (DTG)	56.2 / 53.7	58.6 / 58.2

the DTG module in the OmniVaT with different feature generation methods to generate seven feature nodes, as shown in table 6. Compared with the linear interpolation [21], series generation, and parallel generation [48], our OmniVaT improves at least 1.4% Macro-F1 on the TAG \rightarrow X task. These results indicate that the discrete tree generation can effectively obtain diverse and reliable multimodal fractional representations to reduce the domain gaps.

4) Hyperparameters: We evaluate the influence of the fractional order p and depth R of tree, as shown in fig. 4. We can observe that compared with the original embedding space ($p = 0.0$) and the frequency space ($p = 1.0$), the unified fractional domain space ($p = 0.5$) achieves more effective single domain generalization for multimodal VTL. In addition, when the depth of tree R is set to 3, OmniVaT achieves the best overall performance.

5 Conclusion

In this work, we observe that VTL inherently suffers from both modality and domain gaps, and we propose a new SDG-VTL task towards real-world applications. To address the SDG-VTL task, we propose the first OmniVaT framework for the single VIS-TAC domain generalization. OmniVaT integrates an MFFA module to align VIS-TAC representations within a unified embedding-frequency space, and a DTG module to construct reliable hierarchical fractional features, thus effectively mitigating modality and domain gaps. Experimental results show OmniVaT outperforms SOTA methods in various single domain generalization for multimodal VTL scenarios, demonstrating its effectiveness and robustness. OmniVaT provides a generic blueprint for extending single domain generalization beyond the visual modality to broader multimodal learning. Future work will extend OmniVaT to handle vibrotactile data to overcome the common shortcoming of the existing image-based VTL methods for more comprehensive object understanding.

References

- [1] Shuanghao Bai, Yuedi Zhang, Wanqi Zhou, Zhirong Luan, and Badong Chen. Soft prompt generation for domain generalization. In *Proceedings of the European Conference on Computer Vision*, pages 434–450, 2024. 6, 7, 13, 14

- [2] Berk Calli, Arjun Singh, Aaron Walsman, Siddhartha Srinivasa, Pieter Abbeel, and Aaron M Dollar. The ycb object and model set: Towards common benchmarks for manipulation research. In *Proceedings of the International Conference on Advanced Robotics*, pages 510–517, 2015. 11
- [3] Cagatay Candan, M Alper Kutay, and Haldun M Ozaktas. The discrete fractional fourier transform. *IEEE Transactions on Signal Processing*, 48(5):1329–1337, 2000. 11
- [4] Jin Chen, Zhi Gao, Xinxiao Wu, and Jiebo Luo. Meta-causal learning for single domain generalization. In *Proceedings of the IEEE Conference on Computer Vision and Pattern Recognition*, pages 7683–7692, 2023. 1, 2
- [5] Linwei Chen, Ying Fu, Lin Gu, Chenggang Yan, Tatsuya Harada, and Gao Huang. Frequency-aware feature fusion for dense image prediction. *IEEE Transactions on Pattern Analysis and Machine Intelligence*, 2024. 7
- [6] Maoyang Chen, Shou Feng, Chunhui Zhao, Bo Qu, Nan Su, Wei Li, and Ran Tao. Fractional fourier based frequency-spatial-spectral prototype network for agricultural hyperspectral image open-set classification. *IEEE Transactions on Geoscience and Remote Sensing*, 2024. 2, 3
- [7] Yaxiong Chen, Qicong Wang, Yichen Zhao, Shengwu Xiong, and Xiaoqiang Lu. Bilinear parallel fourier transformer for multimodal remote sensing classification. *IEEE Transactions on Geoscience and Remote Sensing*, 2025. 2
- [8] Junhyeong Cho, Gilhyun Nam, Sungyeon Kim, Hunmin Yang, and Suha Kwak. Promptstyler: Prompt-driven style generation for source-free domain generalization. In *Proceedings of the IEEE International Conference on Computer Vision*, pages 15702–15712, 2023. 3, 4, 6, 7, 8, 13, 14
- [9] Vedant Dave, Fotios Lygerakis, and Elmar Rueckert. Multimodal visual-tactile representation learning through self-supervised contrastive pre-training. In *IEEE International Conference on Robotics and Automation*, pages 8013–8020, 2024. 2, 3
- [10] Elliott Donlon, Siyuan Dong, Melody Liu, Jianhua Li, Edward Adelson, and Alberto Rodriguez. Gelslim: A high-resolution, compact, robust, and calibrated tactile-sensing finger. In *Proceedings of the IEEE/RSJ International Conference on Intelligent Robots and Systems*, pages 1927–1934. IEEE, 2018. 11
- [11] Alexey Dosovitskiy, Lucas Beyer, Alexander Kolesnikov, Dirk Weissenborn, Xiaohua Zhai, Thomas Unterthiner, Mostafa Dehghani, Matthias Minderer, Georg Heigold, Sylvain Gelly, et al. An image is worth 16x16 words: Transformers for image recognition at scale. In *Proceedings of the International Conference on Learning Representations*, 2020. 6, 7, 8, 13, 14
- [12] Ruoxuan Feng, Jiangyu Hu, Wenke Xia, Tianci Gao, Ao Shen, Yuhao Sun, Bin Fang, and Di Hu. Anytouch: Learning unified static-dynamic representation across multiple visuo-tactile sensors. In *Proceedings of the International Conference on Learning Representations*, 2025. 1, 2, 3, 6, 11, 12
- [13] Ruohan Gao, Yiming Dou, Hao Li, Tanmay Agarwal, Jeannette Bohg, Yunzhu Li, Li Fei-Fei, and Jiajun Wu. The objectfolder benchmark: Multisensory learning with neural and real objects. In *Proceedings of the IEEE Conference on Computer Vision and Pattern Recognition*, pages 17276–17286, 2023. 6, 11, 12
- [14] Ruohan Gao, Zilin Si, Yen-Yu Chang, Samuel Clarke, Jeannette Bohg, Li Fei-Fei, Wenzhen Yuan, and Jiajun Wu. Objectfolder 2.0: A multisensory object dataset for sim2real transfer. In *Proceedings of the IEEE Conference on Computer Vision and Pattern Recognition*, pages 10598–10608, 2022. 1, 2, 6, 11, 12
- [15] Hariseetharam Gunduboina, Muhammad Haris Khan, and Biplob Banerjee. Frogdognet: Fourier frequency retained visual prompt output guidance for domain generalization of clip in remote sensing. In *Proceedings of the IEEE Conference on Computer Vision and Pattern Recognition Conference*, pages 2359–2372, 2025. 3
- [16] Yuncheng Guo and Xiaodong Gu. Mmrl: Multi-modal representation learning for vision-language models. In *Proceedings of the IEEE Conference on Computer Vision and Pattern Recognition Conference*, pages 25015–25025, 2025. 6, 7, 13, 14
- [17] Harsh Gupta, Yuchen Mo, Shengmiao Jin, and Wenzhen Yuan. Sensor-invariant tactile representation. In *Proceedings of the International Conference on Learning Representations*, 2025. 1, 2, 6
- [18] Kaiming He, Xiangyu Zhang, Shaoqing Ren, and Jian Sun. Deep residual learning for image recognition. In *Proceedings of the IEEE Conference on Computer Vision and Pattern Recognition*, pages 770–778, 2016. 6
- [19] GelSight. Inc. GelSight Mini, 2022. 11
- [20] Zhong Ji, Zhilong Wang, Xiyao Liu, Yunlong Yu, Yanwei Pang, and Jungong Han. Frequency-spatial complementation: Unified channel-specific style attack for cross-domain few-shot learning. *IEEE Transactions on Image Processing*, 2025. 3
- [21] Byungsoo Ko and Geonmo Gu. Embedding expansion: Augmentation in embedding space for deep metric learning. In *Proceedings of the IEEE Conference on Computer Vision and Pattern Recognition*, pages 7255–7264, 2020. 3, 4, 8
- [22] Emirhan Koç, Tuna Alikasıfoğlu, Arda Can Aras, and Aykut Koç. Trainable fractional fourier transform. *IEEE Signal Processing Letters*, 31:751–755, 2024. 2, 3
- [23] Mike Lambeta, Po-Wei Chou, Stephen Tian, Brian Yang, Benjamin Maloon, Victoria Rose Most, Dave Stroud, Raymond Santos, Ahmad Byagowi, Gregg Kammerer, et al. Digit: A novel design for a low-cost compact high-resolution tactile sensor with application to in-hand manipulation. *IEEE Robotics and Automation Letters*, 5(3):3838–3845, 2020. 11
- [24] Baojiang Li, Jibo Bai, Shengjie Qiu, Haiyan Wang, and Yuting Guo. Vito-transformer: a visual-tactile fusion network for object recognition. *IEEE Transactions on Instrumentation and Measurement*, 2023. 2
- [25] Shuo Li, Fang Liu, Zehua Hao, Xinyi Wang, Lingling Li, Xu Liu, Puhua Chen, and Wenping Ma. Logits deconfusion with clip for few-shot learning. In *Proceedings of the IEEE Conference on Computer Vision and Pattern Recognition Conference*, pages 25411–25421, 2025. 6, 7, 13, 14
- [26] Songhua Liu, Xin Jin, Kingyi Yang, Jingwen Ye, and Xinchao Wang. Stydesty: Min-max stylization and destylization for single domain generalization. *Proceedings of the International Conference on Machine Learning*, 2024. 1, 2, 3
- [27] Ilya Loshchilov and Frank Hutter. Sgdr: Stochastic gradient descent with warm restarts. In *Proceedings of the International Conference on Learning Representations*, 2017. 6
- [28] Wang Lu, Jindong Wang, Haoliang Li, Yiqiang Chen, and Xing Xie. Domain-invariant feature exploration for domain generalization. *Transactions on Machine Learning Research*, 2022. 3

- [29] Xupeng Miao, Gabriele Oliaro, Zhihao Zhang, Xinhao Cheng, Zeyu Wang, Zhengxin Zhang, Rae Ying Yee Wong, Alan Zhu, Lijie Yang, Xiaoxiang Shi, et al. Specinfer: Accelerating large language model serving with tree-based speculative inference and verification. In *Proceedings of the ACM International Conference on Architectural Support for Programming Languages and Operating Systems*, pages 932–949, 2024. 4
- [30] Maxime Oquab, Timothée Darcet, Théo Moutakanni, Huy Vo, Marc Szafraniec, Vasil Khalidov, Pierre Fernandez, Daniel Haziza, Francisco Massa, Alaaeldin El-Nouby, et al. Dinov2: Learning robust visual features without supervision. *arXiv preprint arXiv:2304.07193*, 2023. 1
- [31] Alec Radford, Jong Wook Kim, Chris Hallacy, Aditya Ramesh, Gabriel Goh, Sandhini Agarwal, Girish Sastry, Amanda Askell, Pamela Mishkin, Jack Clark, et al. Learning transferable visual models from natural language supervision. In *Proceedings of the International Conference on Machine Learning*, pages 8748–8763, 2021. 1, 3, 4, 6, 7, 8, 13, 14
- [32] Zilin Si and Wenzhen Yuan. Taxim: An example-based simulation model for gelsight tactile sensors. *IEEE Robotics and Automation Letters*, 7(2):2361–2368, 2022. 1, 11
- [33] Fuyang Wei, Jianhui Zhao, Chudong Shan, and Zhiyong Yuan. Alignment and multi-scale fusion for visual-tactile object recognition. In *Proceedings of the IEEE International Joint Conference on Neural Networks*, pages 1–8, 2022. 2
- [34] Qinwei Xu, Ruipeng Zhang, Ya Zhang, Yanfeng Wang, and Qi Tian. A fourier-based framework for domain generalization. In *Proceedings of the IEEE Conference on Computer Vision and Pattern Recognition*, pages 14383–14392, 2021. 3
- [35] Xiusheng Xu, Lei Qi, Jingyang Zhou, and Xin Geng. Batstyler: Advancing multi-category style generation for source-free domain generalization. *IEEE Transactions on Circuits and Systems for Video Technology*, 2025. 3
- [36] Zhipeng Xu, De Cheng, Xinyang Jiang, Nannan Wang, Dongsheng Li, and Xinbo Gao. Adversarial domain prompt tuning and generation for single domain generalization. In *Proceedings of the IEEE Conference on Computer Vision and Pattern Recognition Conference*, pages 18584–18595, 2025. 1, 2, 3
- [37] Fengyu Yang, Chao Feng, Ziyang Chen, Hyungseob Park, Daniel Wang, Yiming Dou, Ziyao Zeng, Xien Chen, Rit Gangopadhyay, Andrew Owens, et al. Binding touch to everything: Learning unified multimodal tactile representations. In *Proceedings of the IEEE Conference on Computer Vision and Pattern Recognition*, pages 26340–26353, 2024. 1
- [38] Fengyu Yang, Chenyang Ma, Jiacheng Zhang, Jing Zhu, Wenzhen Yuan, and Andrew Owens. Touch and go: Learning from human-collected vision and touch. In *Proceedings of the Advances in Neural Information Processing Systems*, 2022. 1, 2, 3, 6, 11, 12
- [39] Lei Yang. Discrete distribution networks. In *Proceedings of the International Conference on Learning Representations*, 2025. 4
- [40] Shunyu Yao, Dian Yu, Jeffrey Zhao, Izhak Shafran, Tom Griffiths, Yuan Cao, and Karthik Narasimhan. Tree of thoughts: Deliberate problem solving with large language models. *Proceedings of the Advances in Neural Information Processing Systems*, 36:11809–11822, 2023. 4
- [41] Hu Yu, Jie Huang, Lingzhi Li, Feng Zhao, et al. Deep fractional fourier transform. *Proceedings of the Advances in Neural Information Processing Systems*, 36:72761–72773, 2023. 2, 3
- [42] Wenzhen Yuan, Siyuan Dong, and Edward H Adelson. Gelsight: High-resolution robot tactile sensors for estimating geometry and force. *Sensors*, 17(12):2762, 2017. 1, 11
- [43] Chaofan Zhang, Peng Hao, Xiaoge Cao, Xiaoshuai Hao, Shaowei Cui, and Shuo Wang. Vtla: Vision-tactile-language-action model with preference learning for insertion manipulation. *arXiv preprint arXiv:2505.09577*, 2025. 1
- [44] Haoran Zhang, Shuanghao Bai, Wanqi Zhou, Jingwen Fu, and Badong Chen. Promptta: Prompt-driven text adapter for source-free domain generalization. In *Proceedings of the IEEE International Conference on Acoustics, Speech and Signal Processing*, pages 1–5, 2025. 3
- [45] Lunwei Zhang, Yue Wang, and Yao Jiang. Tac3d: A novel vision-based tactile sensor for measuring forces distribution and estimating friction coefficient distribution. *arXiv preprint arXiv:2202.06211*, 2022. 1, 11
- [46] Rouqi Zhang, Chengdi Lu, Hancheng Lu, Yang Cao, and Tiesong Zhao. Robustvish: Robust visual-haptic cross-modal recognition under transmission interference. In *Proceedings of the ACM International Conference on Multimedia*, 2025. 2, 3, 6
- [47] Shixin Zhang, Yiyong Yang, Fuchun Sun, Lei Bao, Jianhua Shan, Yuan Gao, and Bin Fang. A compact visuo-tactile robotic skin for micron-level tactile perception. *IEEE Sensors Journal*, 24(9):15273–15282, 2024. 11
- [48] Yukang Zhang and Hanzi Wang. Diverse embedding expansion network and low-light cross-modality benchmark for visible-infrared person re-identification. In *Proceedings of the IEEE Conference on Computer Vision and Pattern Recognition*, pages 2153–2162, 2023. 3, 4, 8
- [49] Yukang Zhang, Hanzi Wang, Yang Lu, Yan Yan, and Xuelong Li. Frequency domain nuances mining for visible-infrared person re-identification. *IEEE Transactions on Information Forensics and Security*, 20:5411–5424, 2025. 2, 3, 4
- [50] Xudong Zhao, Mengmeng Zhang, Ran Tao, Wei Li, Wenzhi Liao, and Wilfried Philips. Cross-domain classification of multisource remote sensing data using fractional fusion and spatial-spectral domain adaptation. *IEEE Journal of Selected Topics in Applied Earth Observations and Remote Sensing*, 15:5721–5733, 2022. 3
- [51] Xudong Zhao, Mengmeng Zhang, Ran Tao, Wei Li, Wenzhi Liao, Lianfang Tian, and Wilfried Philips. Fractional fourier image transformer for multimodal remote sensing data classification. *IEEE Transactions on Neural Networks and Learning Systems*, 35(2):2314–2326, 2022. 2, 3
- [52] Guangtao Zheng, Mengdi Huai, and Aidong Zhang. Advst: Revisiting data augmentations for single domain generalization. In *Proceedings of the AAAI conference on artificial intelligence*, pages 21832–21840, 2024. 1, 2, 3
- [53] Youjie Zhou, Guofeng Mei, Yiming Wang, Yi Wan, and Fabio Poiesi. Multimodal fusion slam with fourier attention. *IEEE Robotics and Automation Letters*, 10(2):1050–1057, 2025. 2

A More Fractional Fourier Transform Details

The p -th order Fractional Fourier Transform (FrFT) of the embedding $\mathbf{E} \in \mathbb{R}^{1 \times D}$, is defined as follows:

$$\text{FrFT}_p(\mathbf{E}(u_0)) = \int_{-\infty}^{\infty} K_p(u_0, u_p) \mathbf{E}(u_0) du_0, \quad (13)$$

where $K_p(u_0, u_p)$ is the kernel function of the fractional Fourier transform, which can be seen in table 7, u_0 and u_p represent the original embedding space and fractional space, respectively. Although eq. (13) defines the continuous FrFT, practical embeddings are discrete signals. Therefore, we employ the discrete FrFT (DFrFT) [3], that is

$$\mathbf{E}(u_p)[m] = \sum_{n=1}^D \mathbf{F}_p[m, n] \mathbf{E}(u_0)[n], m = 1, \dots, D \quad (14)$$

where $\mathbf{F}_p[m, n] = \sum_{k=1}^D v_k(m) (\lambda_k)^p v_k(n)$ is the discrete FrFT matrix [3], v_k is the k -th discrete Hermite-Gaussians vector, and λ_k represents the corresponding eigenvalues. The final p -order discrete FrFT of embedding \mathbf{E} can be achieved as $\mathbf{E}(u_p) = \mathbf{F}_p \mathbf{E}$.

Table 7 Kernel function $K_p(u_0, u_p)$ of the Fractional Fourier Transform (FrFT) under different α values ($\alpha = p\pi/2$). $A_\alpha = \sqrt{(1 - j \cot \alpha)/2\pi}$ and $\delta(\cdot)$ is the Dirac delta function.

Kernel Expression $K_p(u_0, u_p)$	Condition
$A_\alpha \exp j (u_0^2 \cot \alpha/2 - u_p u_0 \csc \alpha + u_p^2 \cot \alpha/2)$	$\alpha \neq n\pi$
$\delta(u_0 - u_p)$	$\alpha = 2n\pi$
$\delta(u_0 + u_p)$	$\alpha = (2n + 1)\pi$

B More OmniVaT Details

The training and inference processes of the proposed OmniVaT are summarized in algorithms 1 and 2, respectively.

C More Dataset and Task Details

On the Touch-and-Go (TAG) dataset [38], TAC data are captured by the GelSight sensor [42]. The OF Real dataset [13] uses the GelSlim sensor [10], while OF 2.0 [14] provides simulated tactile signals generated by Taxim [32]. We denote the first 100 objects in the OF 2.0 dataset as OF 2.0 A, which are sourced from 3D Model Haven, YCB [2], and Google Scanned Objects, while the remaining objects are referred to as OF 2.0 B. The TacQuad (TQ) dataset [12] includes four tactile sensors: DIGIT [23], GelSight Mini [19], DuraGel [47], and Tac3D [45], yielding the TQ-DIGIT, TQ-GelMini, TQ-DuraGel, and TQ-T3D domains. Dataset statistics are summarized in table 8. Since OF 2.0 A and OF 2.0 B share the same Taxim-based TAC modality, we do not evaluate across them to avoid domain leakage. Because TQ domains do not

Algorithm 1 Training process of OmniVaT.

- 1: **Input:** Single source VIS-TAC domain $\mathcal{S} = \{x^v, x^t, y\}$ with auxiliary LANG information x^l ; initial parameters θ of OmniVaT; epochs H ; mini-batch size B .
 - 2: **Output:** The final parameters θ' of OmniVaT.
 - 3: **for** $h = 1$ to H **do**
 - 4: **for** each mini-batch $\{x^v, x^t, x^l\}_b^B$ in \mathcal{S} **do**
 - 5: Obtain the VIS, TAC, and LANG embeddings by the frozen multimodal encoders.
 - 6: Apply the MFFA module to map multimodal VIS, TAC, and LANG embeddings into the unified embedding-frequency space to mitigate the modality gap via Eqs. (3-6).
 - 7: Apply the DTG module to obtain the diverse and reliable features \mathbf{T}^{tree} for improving the domain generalization ability of the model.
 - 8: Compute the joint loss via Eq. (12).
 - 9: Update θ by stochastic gradient descent.
 - 10: **end for**
 - 11: **end for**
-

Algorithm 2 Inference process of OmniVaT.

- 1: **Input:** Unseen target VIS-TAC domains $\mathcal{T} = \{x^v, x^t\}$; the final parameters θ' of OmniVaT.
 - 2: **Output:** The predicted class of the unseen VIS-TAC sample.
 - 3: **for** each $\{x^v, x^t\}$ in \mathcal{T} **do**
 - 4: Obtain the VIS and TAC embeddings by the frozen multimodal encoders.
 - 5: Apply the MFFA module to map multimodal VIS and TAC embeddings into the unified embedding-frequency space and improve cross-modal semantic consistency.
 - 6: Compute the class probability from the multimodal fractional features.
 - 7: **end for**
-

include ceramic objects, we exclude ceramic samples when constructing unseen domains. Furthermore, when training on TQ domains, we partition it into indoor and outdoor series so that the model is trained and evaluated on non-overlapping data. The SDG-VTL settings are detailed in table 9.

D More Ablation Studies

1) Effectiveness of the Global Class token: As shown in table 10, the global class token brings improvements to OmniVaT. Specifically, OmniVaT with the global class token outperforms its counterpart without it by 0.2% and 0.5% in Macro-F1 on the TAG \rightarrow X and OF 2.0 A \rightarrow X tasks, respectively. This shows that the global class token can reduce intra-class variation and improve SDG-VTL performance.

2) Hyperparameters: fig. 5 illustrates the variations in accu-

Table 8 Summarization of the datasets (domains). Each dataset (domain) provides VIS-TAC samples.

	Domains	TAC Sensors	Training Set	Test Set
	TAG [38]	GelSight	5,520	1,770
	OF Real [13]	GelSlim	3,401	1,355
	OF 2.0 A [14]	Taxim	1,000	2,200
	OF 2.0 B [14]	Taxim	9,500	2,500
<i>TQ Indoor-Outdoor Series</i>				
	TQ-DIGIT [12]	DIGIT	-	810
	TQ-GelMini [12]	GelSight Mini	-	810
	TQ-DuraGel [12]	DuraGel	-	810
<i>TQ Indoor Series</i>				
	TQ-DIGIT (Indoor) [12]	DIGIT	-	525
	TQ-GelMini (Indoor) [12]	GelSight Mini	-	525
	TQ-DuraGel (Indoor) [12]	DuraGel	-	525
	TQ-T3D (Indoor) [12]	Tac3D	1,196	682
<i>TQ Outdoor Series</i>				
	TQ-DIGIT (Outdoor) [12]	DIGIT	779	285
	TQ-GelMini (Outdoor) [12]	GelSight Mini	779	285
	TQ-DuraGel (Outdoor) [12]	DuraGel	779	285

Table 9 The settings of the single domain generalization for multi-modal VIS-TAC learning (SDG-VTL) task.

Seen Domain	Unseen Domains
TAG [38]	OF Real [13], OF 2.0 A [14], OF 2.0 B [14], TQ-DIGIT [12], TQ-GelMini [12], TQ-DuraGel [12], TQ-T3D [12]
OF Real [13]	TAG [38], OF 2.0 A [14], OF 2.0 B [14], TQ-DIGIT [12], TQ-GelMini [12], TQ-DuraGel [12], TQ-T3D [12]
OF 2.0 A [14]	TAG [38], OF Real [13], TQ-DIGIT [12], TQ-GelMini [12], TQ-DuraGel [12], TQ-T3D [12]
OF 2.0 B [14]	TAG [38], OF Real [13], TQ-DIGIT [12], TQ-GelMini [12], TQ-DuraGel [12], TQ-T3D [12]
TQ-DIGIT [12] (Outdoor)	TAG [38], OF Real [13], OF 2.0 A [14], OF 2.0 B [14], TQ-GelMini (Indoor) [12], TQ-DuraGel (Indoor) [12], TQ-T3D (Indoor) [12]
TQ-GelMini [12] (Outdoor)	TAG [38], OF Real [13], OF 2.0 A [14], OF 2.0 B [14], TQ-DIGIT (Indoor) [12], TQ-DuraGel (Indoor) [12], TQ-T3D (Indoor) [12]
TQ-DuraGel [12] (Outdoor)	TAG [38], OF Real [13], OF 2.0 A [14], OF 2.0 B [14], TQ-DIGIT (Indoor) [12], TQ-GelMini (Indoor) [12], TQ-T3D (Indoor) [12]
TQ-T3D [12] (Indoor)	TAG [38], OF Real [13], OF 2.0 A [14], OF 2.0 B [14], TQ-DIGIT (Outdoor) [12], TQ-GelMini (Outdoor) [12], TQ-DuraGel (Outdoor) [12]

Table 10 The influence of the global class token of the proposed OmniVaT on the source TAG and OF 2.0 A domains, respectively. The metrics are accuracy (ACC, %) and Macro-F1 (F1*, %).

Methods	TAG \rightarrow X	OF 2.0 A \rightarrow X
	ACC / F1*	ACC / F1*
Baseline	51.7 / 40.6	48.9 / 41.2
OmniVaT (w/o global class token)	55.8 / 53.5	58.3 / 57.7
OmniVaT (w global class token)	56.2 / 53.7	58.6 / 58.2

racy and Macro-F1 with respect to the extension parameter E and the balance weight λ on the TAG \rightarrow X task. It can be observed that the optimal performance is obtained when $E = 4$ and $\lambda = 10$.

E More Comparison Results

tables 11 to 18 provide detailed comparisons of OmniVaT and prior SOTA methods on 8 VIS-TAC domains. Overall, OmniVaT achieves the highest average performance. This

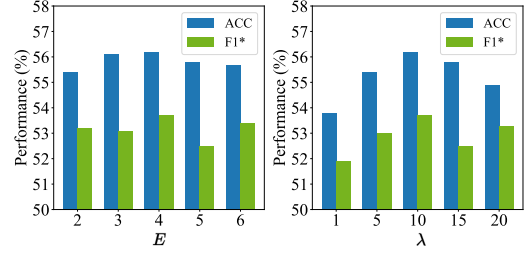


Figure 5 The influence of the extension parameter E and the balance weight λ on the TAG \rightarrow X task.

demonstrates that our OmniVaT is able to achieve more effective single-domain generalization for VIS-TAC learning.

Table 11 Comparison with state-of-the-art methods on the TAG \rightarrow X task. “TAG \rightarrow X” represents the evaluation of the other unseen target domains, excluding the seen source TAG domain. Δ LDC denotes the improvements of the proposed OmniVaT over LDC. The metrics are accuracy (ACC, %) and Macro-F1 (F1*, %).

Methods / Venue	\rightarrow OF Real	\rightarrow OF 2.0 A	\rightarrow OF 2.0 B	\rightarrow TQ-DIGIT	\rightarrow TQ-GelMini	\rightarrow TQ-DuraGel	\rightarrow TQ-T3D	Average
	ACC / F1*	ACC / F1*	ACC / F1*	ACC / F1*	ACC / F1*	ACC / F1*	ACC / F1*	ACC / F1*
<i>ViT-B / 16 [11] with pre-trained weights from CLIP [31]</i>								
CLIP / ICML-21 [31]	49.0 / 48.8	51.6 / 37.5	48.1 / 46.0	37.3 / 32.6	47.5 / 31.8	44.4 / 31.8	56.9 / 51.5	47.8 / 40.0
PromptStyler / ICCV-23 [8]	47.5 / 37.4	46.0 / 24.8	43.3 / 22.4	59.3 / 58.9	53.8 / 46.8	53.6 / 49.3	58.4 / 44.4	51.7 / 40.6
SPG / ECCV-24 [1]	46.3 / 37.3	39.5 / 19.9	38.4 / 27.2	52.8 / 52.4	55.9 / 55.5	54.7 / 43.0	58.2 / 57.8	49.4 / 41.9
MMRL / CVPR-25 [16]	37.4 / 24.7	37.5 / 18.0	26.7 / 17.4	53.1 / 46.6	56.0 / 49.1	54.4 / 52.5	57.1 / 26.4	46.0 / 33.5
LDC / CVPR-25 [25]	51.2 / 36.0	43.8 / 27.6	41.2 / 34.1	49.4 / 47.6	53.8 / 44.8	54.2 / 33.6	57.1 / 30.1	50.1 / 36.3
OmniVaT / Ours	56.7 / 50.8	52.3 / 38.1	48.7 / 46.7	61.3 / 60.0	58.7 / 60.4	56.1 / 59.2	59.3 / 60.5	56.2 / 53.7
Δ LDC	5.5 / 14.8	8.5 / 10.5	7.5 / 12.6	11.9 / 12.4	4.9 / 15.6	1.9 / 25.6	2.2 / 30.4	6.1 / 17.4

Table 12 Comparison with state-of-the-art methods on the OF Real \rightarrow X task. “OF Real \rightarrow X” represents the evaluation of the other unseen target domains, excluding the seen source OF Real domain. Δ LDC denotes the improvements of the proposed OmniVaT over LDC. The metrics are accuracy (ACC, %) and Macro-F1 (F1*, %).

Methods / Venue	\rightarrow TAG	\rightarrow OF 2.0 A	\rightarrow OF 2.0 B	\rightarrow TQ-DIGIT	\rightarrow TQ-GelMini	\rightarrow TQ-DuraGel	\rightarrow TQ-T3D	Average
	ACC / F1*	ACC / F1*	ACC / F1*	ACC / F1*	ACC / F1*	ACC / F1*	ACC / F1*	ACC / F1*
<i>ViT-B / 16 [11] with pre-trained weights from CLIP [31]</i>								
CLIP / ICML-21 [31]	51.4 / 49.8	51.6 / 37.5	48.1 / 46.0	37.3 / 32.6	47.5 / 31.8	44.4 / 31.8	56.9 / 51.5	48.2 / 40.1
PromptStyler / ICCV-23 [8]	38.7 / 34.0	45.1 / 34.3	39.6 / 32.0	47.0 / 26.8	42.1 / 25.4	42.0 / 24.1	41.8 / 34.4	42.3 / 30.1
SPG / ECCV-24 [1]	54.7 / 39.9	49.8 / 34.9	33.4 / 26.6	47.1 / 41.4	61.3 / 51.1	43.8 / 48.1	58.3 / 52.3	49.8 / 42.0
MMRL / CVPR-25 [16]	44.4 / 37.9	36.9 / 32.4	32.7 / 34.0	44.3 / 43.7	53.7 / 60.8	49.5 / 42.5	59.5 / 66.5	45.9 / 45.4
LDC / CVPR-25 [25]	41.5 / 39.1	52.8 / 39.3	46.7 / 40.0	42.3 / 32.9	50.9 / 33.1	57.8 / 39.7	54.7 / 39.2	49.5 / 37.6
OmniVaT / Ours	67.9 / 66.1	51.8 / 34.9	47.3 / 40.2	61.6 / 64.5	62.9 / 62.6	56.3 / 58.9	60.7 / 68.1	58.4 / 56.5
Δ LDC	26.4 / 27.0	-1.0 / -4.4	0.6 / 0.2	19.3 / 31.6	12.0 / 29.5	-1.5 / 19.2	6.0 / 28.9	8.9 / 18.9

Table 13 Comparison with state-of-the-art methods on the OF 2.0 A \rightarrow X task. “OF 2.0 A \rightarrow X” represents the evaluation of the other unseen target domains, excluding the seen source OF 2.0 A domain. Δ LDC denotes the improvements of the proposed OmniVaT over LDC. The metrics are accuracy (ACC, %) and Macro-F1 (F1*, %).

Methods / Venue	\rightarrow TAG	\rightarrow OF Real	\rightarrow TQ-DIGIT	\rightarrow TQ-GelMini	\rightarrow TQ-DuraGel	\rightarrow TQ-T3D	Average
	ACC / F1*	ACC / F1*	ACC / F1*	ACC / F1*	ACC / F1*	ACC / F1*	ACC / F1*
<i>ViT-B / 16 [11] with pre-trained weights from CLIP [31]</i>							
CLIP / ICML-21 [31]	51.4 / 49.8	49.0 / 48.8	37.3 / 32.6	47.5 / 31.8	44.4 / 31.8	56.9 / 51.5	47.8 / 41.1
PromptStyler / ICCV-23 [8]	49.4 / 43.0	48.6 / 37.0	40.4 / 29.4	55.0 / 50.7	51.8 / 47.5	48.1 / 39.3	48.9 / 41.2
SPG / ECCV-24 [1]	41.3 / 36.0	40.7 / 36.4	57.8 / 46.8	60.4 / 53.3	52.1 / 42.6	42.3 / 41.7	49.1 / 42.8
MMRL / CVPR-25 [16]	39.9 / 27.6	40.9 / 23.6	43.5 / 34.1	42.8 / 39.2	46.4 / 25.4	43.8 / 30.5	42.9 / 30.1
LDC / CVPR-25 [25]	49.2 / 42.5	50.2 / 40.9	51.9 / 47.1	61.4 / 54.3	54.5 / 44.5	46.1 / 33.8	52.2 / 43.9
OmniVaT / Ours	51.0 / 45.5	51.8 / 43.0	64.8 / 66.5	65.1 / 68.2	62.7 / 65.6	56.4 / 60.7	58.6 / 58.2
Δ LDC	1.8 / 3.0	1.6 / 2.1	12.9 / 19.4	3.7 / 13.9	8.2 / 21.1	10.3 / 26.9	6.4 / 14.3

Table 14 Comparison with state-of-the-art methods on the OF 2.0 B \rightarrow X task. “OF 2.0 B \rightarrow X” represents the evaluation of the other unseen target domains, excluding the seen source OF 2.0 B domain. Δ LDC denotes the improvements of the proposed OmniVaT over LDC. The metrics are accuracy (ACC, %) and Macro-F1 (F1*, %).

Methods / Venue	\rightarrow TAG	\rightarrow OF Real	\rightarrow TQ-DIGIT	\rightarrow TQ-GelMini	\rightarrow TQ-DuraGel	\rightarrow TQ-T3D	Average
	ACC / F1*	ACC / F1*	ACC / F1*	ACC / F1*	ACC / F1*	ACC / F1*	ACC / F1*
<i>ViT-B / 16 [11] with pre-trained weights from CLIP [31]</i>							
CLIP / ICML-21 [31]	51.4 / 49.8	49.0 / 48.8	37.3 / 32.6	47.5 / 31.8	44.4 / 31.8	56.9 / 51.5	47.8 / 41.1
PromptStyler / ICCV-23 [8]	33.8 / 27.8	35.2 / 20.9	34.7 / 23.8	32.8 / 17.3	30.8 / 13.5	60.5 / 56.7	38.0 / 26.7
SPG / ECCV-24 [1]	56.8 / 53.0	49.0 / 42.2	53.6 / 45.6	58.2 / 46.0	42.9 / 37.1	35.9 / 27.9	49.4 / 42.0
MMRL / CVPR-25 [16]	49.3 / 44.1	45.5 / 36.6	47.3 / 40.2	47.7 / 46.9	23.6 / 21.8	40.3 / 33.8	42.3 / 37.2
LDC / CVPR-25 [25]	49.2 / 47.9	49.7 / 50.6	51.3 / 41.0	52.4 / 44.2	57.4 / 43.6	53.0 / 35.6	52.2 / 43.8
OmniVaT / Ours	65.0 / 62.6	57.3 / 52.4	59.5 / 60.0	64.1 / 65.1	59.2 / 54.4	62.4 / 67.2	61.2 / 60.3
Δ LDC	15.8 / 14.7	7.6 / 1.8	8.2 / 19.0	11.7 / 20.9	1.8 / 10.8	9.4 / 31.6	9.0 / 16.5

Table 15 Comparison with state-of-the-art methods on the TQ-DIGIT \rightarrow X task. “TQ-DIGIT \rightarrow X” represents the evaluation of the other unseen target domains, excluding the seen source TQ-DIGIT domain. Δ LDC denotes the improvements of the proposed OmniVaT over LDC. The metrics are accuracy (ACC, %) and Macro-F1 (F1*, %).

Methods / Venue	\rightarrow TAG	\rightarrow OF Real	\rightarrow OF 2.0 A	\rightarrow OF 2.0 B	\rightarrow TQ-GelMini	\rightarrow TQ-DuraGel	\rightarrow TQ-T3D	Average
	ACC / F1*	ACC / F1*	ACC / F1*	ACC / F1*	ACC / F1*	ACC / F1*	ACC / F1*	ACC / F1*
<i>ViT-B / 16 [11] with pre-trained weights from CLIP [31]</i>								
CLIP / ICML-21 [31]	53.0 / 40.4	46.7 / 40.6	45.8 / 26.1	41.2 / 33.7	57.3 / 34.1	37.3 / 30.7	56.9 / 51.5	48.3 / 36.7
PromptStyler / ICCV-23 [8]	52.4 / 47.7	61.3 / 50.5	52.0 / 36.8	45.4 / 38.6	58.9 / 53.3	58.6 / 46.7	51.8 / 56.8	54.3 / 47.2
SPG / ECCV-24 [1]	53.4 / 50.8	56.4 / 51.1	49.9 / 37.7	42.4 / 35.7	60.5 / 57.9	55.1 / 45.0	54.1 / 50.0	53.1 / 46.9
MMRL / CVPR-25 [16]	28.4 / 17.3	31.9 / 12.8	27.8 / 10.9	26.8 / 13.5	50.3 / 26.4	46.7 / 23.5	39.9 / 21.1	36.0 / 17.9
LDC / CVPR-25 [25]	53.4 / 51.7	56.1 / 49.6	54.9 / 25.3	44.7 / 33.3	54.9 / 38.6	55.4 / 41.9	57.0 / 32.1	53.8 / 38.9
OmniVaT / Ours	55.7 / 52.2	61.8 / 51.7	57.8 / 36.6	44.3 / 35.2	57.8 / 52.8	58.2 / 63.5	58.9 / 59.0	56.4 / 50.1
Δ LDC	2.3 / 0.5	5.7 / 2.1	2.9 / 11.3	-0.4 / 1.9	2.9 / 14.2	2.8 / 21.6	1.9 / 26.9	2.6 / 11.2

Table 16 Comparison with state-of-the-art methods on the TQ-GelMini \rightarrow X task. “TQ-GelMini \rightarrow X” represents the evaluation of the other unseen target domains, excluding the seen source TQ-GelMini domain. Δ LDC denotes the improvements of the proposed OmniVaT over LDC. The metrics are accuracy (ACC, %) and Macro-F1 (F1*, %).

Methods / Venue	\rightarrow TAG	\rightarrow OF Real	\rightarrow OF 2.0 A	\rightarrow OF 2.0 B	\rightarrow TQ-DIGIT	\rightarrow TQ-DuraGel	\rightarrow TQ-T3D	Average
	ACC / F1*	ACC / F1*	ACC / F1*	ACC / F1*	ACC / F1*	ACC / F1*	ACC / F1*	ACC / F1*
<i>ViT-B / 16 [11] with pre-trained weights from CLIP [31]</i>								
CLIP / ICML-21 [31]	53.0 / 40.4	46.7 / 40.6	45.8 / 26.1	41.2 / 33.7	44.4 / 39.1	37.3 / 30.7	56.9 / 51.5	46.5 / 37.4
PromptStyler / ICCV-23 [8]	35.8 / 33.2	55.7 / 45.2	50.7 / 36.2	44.3 / 37.1	43.3 / 46.2	47.5 / 35.0	52.0 / 45.6	47.0 / 39.8
SPG / ECCV-24 [1]	53.7 / 50.0	56.4 / 48.7	51.2 / 38.0	40.5 / 34.9	60.1 / 57.9	54.5 / 51.5	60.4 / 59.5	53.8 / 48.6
MMRL / CVPR-25 [16]	32.1 / 22.7	32.1 / 12.7	27.8 / 11.0	24.0 / 12.3	11.6 / 8.4	30.7 / 19.7	33.0 / 19.4	27.3 / 15.2
LDC / CVPR-25 [25]	52.9 / 48.5	44.7 / 28.2	47.1 / 32.8	36.4 / 28.0	43.1 / 33.3	41.2 / 33.9	47.6 / 42.2	44.7 / 35.3
OmniVaT / Ours	58.0 / 60.0	61.1 / 49.8	53.6 / 39.8	45.1 / 33.9	64.9 / 69.6	56.3 / 60.5	62.0 / 61.0	57.3 / 53.5
Δ LDC	5.1 / 11.5	16.4 / 21.6	6.5 / 7.0	8.7 / 5.9	21.8 / 36.3	15.1 / 26.6	14.4 / 18.8	12.6 / 18.2

Table 17 Comparison with state-of-the-art methods on the TQ-DuraGel \rightarrow X task. “TQ-DuraGel \rightarrow X” represents the evaluation of the other unseen target domains, excluding the seen source TQ-DuraGel domain. Δ LDC denotes the improvements of the proposed OmniVaT over LDC. The metrics are accuracy (ACC, %) and Macro-F1 (F1*, %).

Methods / Venue	\rightarrow TAG	\rightarrow OF Real	\rightarrow OF 2.0 A	\rightarrow OF 2.0 B	\rightarrow TQ-DIGIT	\rightarrow TQ-GelMini	\rightarrow TQ-T3D	Average
	ACC / F1*	ACC / F1*	ACC / F1*	ACC / F1*	ACC / F1*	ACC / F1*	ACC / F1*	ACC / F1*
<i>ViT-B / 16 [11] with pre-trained weights from CLIP [31]</i>								
CLIP / ICML-21 [31]	53.0 / 40.4	46.7 / 40.6	45.8 / 26.1	41.2 / 33.7	44.4 / 39.1	57.3 / 34.1	37.3 / 30.7	46.5 / 35.0
PromptStyler / ICCV-23 [8]	46.9 / 46.0	58.4 / 47.7	47.9 / 36.6	41.8 / 38.2	54.3 / 59.1	53.4 / 47.5	59.6 / 61.9	51.8 / 48.1
SPG / ECCV-24 [1]	54.0 / 53.1	50.6 / 43.2	38.8 / 34.9	40.7 / 34.6	65.2 / 63.8	56.2 / 44.1	55.5 / 50.2	51.6 / 46.3
MMRL / CVPR-25 [16]	25.0 / 10.6	31.9 / 12.1	27.8 / 11.0	25.0 / 10.0	29.0 / 12.0	36.6 / 26.2	32.1 / 19.0	29.6 / 14.4
LDC / CVPR-25 [25]	53.3 / 51.7	38.4 / 29.8	47.3 / 26.1	43.8 / 25.2	52.6 / 48.4	54.4 / 50.5	54.7 / 36.6	49.2 / 38.3
OmniVaT / Ours	57.2 / 57.0	58.3 / 49.8	47.8 / 39.8	49.3 / 36.9	64.1 / 69.6	56.0 / 49.3	61.2 / 60.0	56.3 / 51.8
Δ LDC	3.9 / 5.3	19.9 / 20.0	0.5 / 13.7	5.5 / 11.7	11.5 / 21.2	1.6 / -1.2	6.5 / 23.4	7.1 / 13.5

Table 18 Comparison with state-of-the-art methods on the TQ-T3D \rightarrow X task. “TQ-T3D \rightarrow X” represents the evaluation of the other unseen target domains, excluding the seen source TQ-T3D domain. Δ LDC denotes the improvements of the proposed OmniVaT over LDC. The metrics are accuracy (ACC, %) and Macro-F1 (F1*, %).

Methods / Venue	\rightarrow TAG	\rightarrow OF Real	\rightarrow OF 2.0 A	\rightarrow OF 2.0 B	\rightarrow TQ-DIGIT	\rightarrow TQ-GelMini	\rightarrow TQ-DuraGel	Average
	ACC / F1*	ACC / F1*	ACC / F1*	ACC / F1*	ACC / F1*	ACC / F1*	ACC / F1*	ACC / F1*
<i>ViT-B / 16 [11] with pre-trained weights from CLIP [31]</i>								
CLIP / ICML-21 [31]	53.0 / 40.4	46.7 / 40.6	45.8 / 26.1	41.2 / 33.7	24.2 / 20.4	29.5 / 27.4	57.5 / 27.3	42.6 / 30.8
PromptStyler / ICCV-23 [8]	52.9 / 48.8	50.7 / 37.1	43.3 / 21.4	44.7 / 26.1	51.0 / 26.0	50.8 / 22.0	52.6 / 35.2	49.4 / 30.9
SPG / ECCV-24 [1]	54.3 / 53.8	46.4 / 42.2	45.4 / 27.8	36.2 / 32.9	59.4 / 48.6	56.8 / 50.1	54.4 / 50.9	50.4 / 43.8
MMRL / CVPR-25 [16]	38.3 / 33.6	56.6 / 46.4	47.5 / 31.1	40.9 / 25.9	53.7 / 37.5	53.9 / 42.9	50.9 / 26.2	48.8 / 34.8
LDC / CVPR-25 [25]	56.1 / 43.2	55.4 / 36.8	46.5 / 21.3	39.2 / 22.5	54.9 / 35.6	58.2 / 42.3	60.2 / 42.4	52.9 / 34.9
OmniVaT / Ours	56.5 / 59.1	58.6 / 49.3	47.1 / 30.2	42.2 / 38.1	57.9 / 50.9	59.2 / 54.7	57.1 / 53.3	54.1 / 47.9
Δ LDC	0.4 / 15.9	3.2 / 12.5	0.6 / 8.9	3.0 / 15.6	3.0 / 15.3	1.0 / 12.4	-3.1 / 10.9	1.2 / 13.0